Histochem Cell Biol
DOI 10.1007/s00418-012-1034-0

ORIGINAL PAPER

Urothelial endocytic vesicle recycling and lysosomal degradative pathway regulated by lipid membrane composition

E. J. Grasso · R. O. Calderón

Accepted: 10 September 2012

Abstract The urothelium, a specialized epithelium that covers the mucosa cell surface of the urinary bladder, undergoes dramatic morphological changes during the micturition cycle that involve a membrane apical traffic. This traffic was first described as a lysosomal pathway, in addition to the known endocytosis/exocytosis membrane recycling. In an attempt to understand the role of membrane lipid composition in those effects, we previously described the lipid-dependent leakage of the endocytosed vesicle content. In this work, we demonstrated clear differences in the traffic of both the fluid probe and the membrane-bound probe in urothelial umbrella cells by using spectrofluorometry and/or confocal and epifluorescence microscopy. Different membrane lipid compositions were established by using three diet formulae enriched in oleic acid, linoleic acid and a commercial formula. Between three and five animals for each dietary treatment were used for each analysis. The decreased endocytosis of both fluid and membrane-bound probes (approximately 32 and 49 % lower, respectively) in oleic acid-derived umbrella cells was concomitant with an increased recycling (approximately 4.0 and 3.7 times, respectively) and diminished sorting to the lysosome (approximately 23 and 37 %, respectively) when compared with the control umbrella cells. The higher intravesicular pH and the impairment of the lysosomal pathway of oleic acid diet-derived vesicles compared to linoleic acid diet-derived vesicles and control diet-derived vesicles correlate with our findings of a lower V-ATPase activity previously reported. We integrated the results obtained in the present and previous work to determine the sorting of endocytosed material (fluid and membrane-bound probes) into the different cell compartments. Finally, the weighted average effect of the individual alterations on the intracellular distribution was evaluated. The results shown in this work add evidences for the modulatory role of the membrane lipid composition on sorting of the endocytosed material. This suggests that changes in the membrane organization can be one of the underlying mechanisms for regulating the endocytosis/exocytosis processes and membrane intracellular trafficking.

Keywords Fatty acids · Urothelial endocytic vesicles · Recycling pathway · Lysosomal degradative pathway · Endocytotic capacity

E. J. Grasso
Centro de Investigaciones en Química Biológica de Córdoba (CIQUIBIC), Consejo Nacional de Investigaciones Científicas y Tecnológicas (CONICET), Universidad Nacional de Córdoba, CP5000, CC220 Ciudad Universitaria, Córdoba, Argentina

R. O. Calderón (✉)
Cátedra de Biología Celular, H. y E., Instituto de Biología Celular-Facultad de Ciencias Médicas, Universidad Nacional de Córdoba, CP5000, CC220 Ciudad Universitaria, Córdoba, Argentina
e-mail: olga@cmefcm.uncor.edu

Introduction

The urothelium is a specialized epithelium covering the mucosal cell surface of the urinary bladder. It is composed of three cell layers: basal, intermediate and superficial or umbrella cells which are in direct contact with urine (Lewis 2000). The umbrella cells are distinguished by two unique structural features: the urothelial plaques and the high density of fusiform vesicles (Lewis 2000; Zhou et al. 2012). A traffic model of fusiform vesicles was originally proposed by Hicks (1975) that basically supports the

Published online: 12 October 2012

increase and decrease of urothelium luminal surface during filling and voiding, respectively, of the micturition cycle. According to it, the vesicles formed by endocytosis and located beneath the apical plasma membrane are exocytosed (recycled) in response to the increase of membrane tension during the filling phase (Lewis 2000; Apodaca 2004). Nevertheless, in the last decade, new evidences have demonstrated alternative endocytotic pathways of both membrane and fluid phases. Zhang and Seguchi reported evidences of the vesicle pathway toward the lysosomal degradation by showing the surface characteristic of urothelial plaques in multivesicular bodies, autophagosomes and lysosomes of umbrella cells (Zhang and Seguchi 1994). Truschel et al. (2002) have also reported that once the vesicles have been endocytosed, their membrane protein content, specifically the uroplakin III, could be degraded via lysosomes. Guo et al. (2009) have recently demonstrated the acidification of the endocytic vesicle content and its dependence on Vps33a, a Sec-1 related protein implicated in vesicular transport to the lysosomal compartment. Moreover, recent data described at least two kinds of intracellular vesicles: the discoidal/fusiform vesicles (FVs) and the peripheral junction-associated apical endosomes (Khandelwal et al. 2010). The vesicles associated with peripheral junction proceed by compensatory endocytosis from the apical membrane (Khandelwal et al. 2010) and represent an integrin-regulated and RhoA- and dynamin-dependent pathway. Both membrane and fluid internalized in this way are targeted to lysosomal degradation (Khandelwal et al. 2010) via their delivery to late endosomes, thus avoiding the pathway from FVs to the early endosomes in a non-classical lysosomal pathway. Other authors provided evidence that a membrane-bound endocytotic marker was sorted to early endosome compartment after endocytosis and matured in late endosome and later in lysosome (Kreft et al. 2009). These authors also suggested the dichotomous origin of the vesicles: one class coming from FVs can be regarded as exocytic, rather than endocytic, delivering uroplakins to the apical plasma membrane; and a second class constituted by the endocytic vesicles coming from the hinge membrane regions located between the urothelial plaques (Kreft et al. 2009).

Independent of their origin, the vesicles will eventually be degraded in the lysosome (Truschel et al. 2002; Kreft et al. 2009; Khandelwal et al. 2010). This process requires an acidic pH that activates the lysosomal hydrolytic enzymes. The acidic pH is achieved by a urothelial V-ATPase (Grasso et al. 2011a), composed of two multisubunit domains: the membrane proton channel V_0, responsible for proton translocation, and the peripheral catalytic segment V_1, where ATP hydrolysis occurs. In fact, the proton translocation efficiency or acidification rate is dependent on the coupling of both domains (Cipriano et al. 2008). We described for the first time the correlation between the lipid composition and the V-ATPase function/activity. It was shown how changes of membrane lipid composition of endocytic vesicles could induce a functional uncoupling between both of V-ATPase domains (Grasso et al. 2011a). We demonstrated previously that plasma membrane of the umbrella cells could be modified in its lipid composition by dietary treatments (Calderón et al. 1998). These changes resulted in differential membrane rigidity, determined by fluorescence anisotropy (Calderón and Eynard 2000). We also observed topological alterations of the urothelial plaques: the association between uroplakin dimers (Bongiovanni et al. 2005) and the surface topography of urothelial particles was dependent on membrane lipid composition (Calderón and Grasso 2006). Moreover, we observed that the lipid composition also had an effect on the vesicle membrane permeability, describing for the first time the cytosolic leakage of endocytic vesicles content (Grasso and Calderón 2009). Besides, urothelial V-ATPase activity was modulated by the membrane lipid composition (Grasso et al. 2011a). The observations, previously described, prompted us to investigate whether changes of membrane lipid composition could operate as a sorting signal affecting urothelial vesicle traffic. To this end, in this work we studied the traffic of urothelial endocytic vesicles by determining the endocytosis capability, the recycling cycle and the lysosomal degradation of vesicles with different membrane lipid composition as modified by dietary treatments. Defining the role of membrane lipids on the intracellular traffic is important for understanding the regulation of the whole process of urothelial endocytosis.

Materials and methods

Animals and diets

After weaning, three groups of 25 Wistar rats (both sexes) (3–5 animals were used for each experiment) were fed ad libitum for 12 weeks with semi-synthetic formulae containing (%w/w) 20.0 casein, 50.0 sucrose, 20.0 corn starch, 3.5 salt mixture, 1.0 vitamins mixture, 0.3 methionine, 0.1 choline and 6 % of one of the following lipid sources: corn oil, enriched in 18:2n-6 (linoleic acid); olive oil, enriched in 18:1n-9 (oleic acid). Another group was fed with commercial animal diet (Cargil, Co) and used as a control. Food and water were provided ad libitum. Animals were kept in a light and temperature controlled room under the rules of the Institutional Animal Care Guidelines (Animal Care Committee from National University of Cordoba, Argentina) and were fed fresh diet every day.

Histological analysis

Rats were killed by a lethal anesthesia overdose. Once the animal lost consciousness, we proceeded to open the abdominal cavity and expose the urinary bladder. Rat bladders were clamped in situ, inflated with 200 µL of 4 % paraformaldehyde solution at room temperature, excised and submerged in the same fixation solution. We carefully ensured that the bladder was inflated before the animal's death. After 72 h, the fixative was removed. The rat bladders were embedded in paraffin and sectioned (3-µm thick slides). After deparaffinization and rehydration, the sections were stained with hematoxylin and eosin. The slides were mounted using DPX medium (Sigma, Co) and visualized using a Zeiss Axioskop microscope equipped with an oil immersion objective 100× (numerical aperture = 1.4, Zeiss Plan-Apochromat). The final images were captured on a Zeiss CCD camera and compiled with Adobe Photoshop 7.0.

Fatty acid composition and hydrophobic core structural parameters of urothelial endocytic vesicle membranes

The fatty acid composition of urothelial endocytic vesicles was determined by gas chromatography in a previous work (Grasso et al. 2011a). With those data, we have now determined the structural parameters of endocytic membrane-hydrophobic core as described by Mason et al. (1981). To do this, we calculated four average structural parameters: (1) the chain length of each fatty acid (CL); (2) the "weighted" average chain length (WACL) of *sn-1* and *sn-2* acyl chains; (3) the effective in equivalence (interdigitation) or ΔC between *sn-1* and *sn-2* acyl chains and (4) the membrane-hydrophobic core thickness (HCT). See "Results", "Hydrophobic core structural parameters of urothelial endocytic vesicle membranes".

Fluid-probe endocytosis determination

Spectrofluorometric assays

The ureters and urethra were clamped in situ after bladder exposure. The bladder interior was washed three times with PBS at 37 °C and then filled with 300 µL of 20 mM HPTS (hydroxypyrene-1,3,6-trisulfonic acid, Sigma Co), 22.2 mM glucose, 1.1 H_2KPO_4, 0.4 mM Na_2HPO_4, 5.4 mM KCl and 106 mM NaCl solution, pH 7.5. HPTS is a hydrosoluble fluorescent compound and was used as a fluid-probe marker. After filling, the bladders with their content were excised and incubated for 60 min into a Ringer hypotonic solution (in mM: 111.2 NaCl, 25 $NaHCO_3$, 5.8 KCl, 2 $CaCl_2$, 1.2 $MgSO_4$, 1.2 K_2HPO_4, 11.1 glucose, pH 7.4; diluted 1:1 with distilled water) at 37 °C, which induced the reinsertion of subapical vesicles to the apical surface (Lewis and de Moura 1984). Subsequently, the bladders were changed to an isotonic Ringer solution and left to stand for the indicated time in each case to induce the endocytosis of plasma membrane, forming vesicles containing the entrapped marker. After the hypotonic–isotonic shock, the bladders were cut open and the urothelial cells were obtained by scraping off the luminal surface and collected by centrifugation (800×*g*) followed by three washing with PBS, according to Calderón et al. (1998). The value of endocytosed probe corresponds to the fluorescence released from the umbrella cell suspension loaded with HPTS after cell lysis with 0.02 % Triton X-100. The fluorescence was measured in an SLM-Aminco (Urbana, IL) spectrofluorometer at λ_{em} 510 nm (λ_{exc} 475 nm) after pH adjustment to 7.3. The quantity of endocytosed material was referred to as the fluorescence percentage of the total fluorescence inoculated in the urinary bladder lumen.

Confocal microscopy

We induced the fluid-probe endocytosis as described above. After the hypotonic–isotonic shock, the probe excess was washed out with cold PBS and the urinary bladders were frozen at −20° in a cryostat and 3-µm thick cryosections were obtained. The sections were mounted in positive polylysine-charged slides and fixed with 4 % paraformaldehyde solution at 4 °C. Confocal images were collected using a Carl Zeiss LSM5 Pascal laser scanning confocal microscope (Carl Zeiss AG, Germany) equipped with a multiline argon laser (458, 488 and 514 nm) and two helium–neon lasers (543 and 633 nm respectively) and 100× (numerical aperture = 1.4) oil immersion objective (Zeiss Plan-Apochromat). Single confocal sections of 0.7 µm were taken parallel to the coverslip (*xy* sections). Images were compiled with Adobe Photoshop 7. The fluorescence intensity was measured by using the software Sigma Scan Pro 5.0 (Spss Inc. 1987–1999).

Membrane-bound probe endocytosis determination

In this case, prior to the endocytosis induction, the urothelial surface was labeled by filling the bladder with a rabbit IgG anti-uroplakin III (1:100) prepared in our laboratory (Bongiovanni et al. 2005). This antibody was used as a membrane-bound probe marker. After filling, the bladders with their content were excised and incubated for 30 min into a Ringer hypotonic solution at 37 °C. Then, the antibody excess was removed and the bladders were filled with an anti-rabbit IgG conjugated with FITC (1:100, λ_{exc} 490 λ_{em} 515, Sigma Co) and incubated for 30 min in the same Ringer hypotonic solution. At the end of the immunostaining, endocytosis of the membrane probe was induced by changing the bladders to an isotonic Ringer

solution and allowing to stand for the indicated time in each case. After endocytosis induction, the lumen of the bladders was washed once with PBS 0.5 % acetic acid for 1 min to remove the non-endocytosed probe. The urothelial cells loaded with the endocytosed probes were isolated and the fluorescence was measured by spectrofluorometric assays and confocal microscopy as described in the previous section.

Endocytic vesicles pH measurements

Vesicle isolation

To isolate the endocytic vesicles after HPTS endocytosis induction, as described in "Fluid-probe endocytosis determination", the bladders were cut open in a Petri dish placed on ice and the urothelium was obtained by scraping the luminal surface, collected by centrifugation and mechanically disrupted in the homogenization solution (in mM: 10 N-2-hydroxyethylpiperazine-N-2-ethanesulfonic acid, 10 KCl, 45 sucrose, 1 EDTA, 1 ethylene glycol-bis (2-aminoethylether)-N,N,N′,N′-tetraacetic acid, pH 8). The disrupted tissue was layered over a 1.6 M sucrose cushion (Chang et al. 1994; Grasso and Calderón 2009) and centrifuged at 28,000×*g* at 4 °C for 20 min in an L5-50B Beckman Ultracentrifuge. The vesicle-enriched fraction was collected at the water–sucrose interface and immediately assayed (SLM-Aminco spectrofluorometer). The integrity of the loaded vesicles was always tested by treatment of a separate aliquot with Triton X-100 (0.2 %) and measuring the increase of fluorescence upon dilution that follows the release of the trapped self-quenched pH-sensitive probe. A calibration curve of fluorescence emission intensity ratios (λ_{exc} 405 and λ_{exc} 470 nm) as a function of pH was constructed using the fluorescence spectra of HPTS (Straubinger et al. 1990). All fluorescence measurements (arbitrary units, AU) were normalized to 100 μg protein.

Epifluorescence microscopy

The umbrella cells were loaded with HPTS and isolated as described in "Fluid-probe endocytosis determination". HPTS fluorescence was viewed using a Zeiss Axioplan fluorescence microscopy (Carl Zeiss, Germany) equipped with a UV radiation source provided by a mercury HBO-50 lamp and a fluorescence 40× objective (NA = 1.4, Zeiss Plan-Apochromat). The pH-independent fluorescence of HPTS was viewed with a 01 Zeiss filter set (violet, λ_{exc} 365–412 nm). The 09 filter set (blue, λ_{exc} 450–490 nm) was used for viewing the HPTS fluorescence at neutral or basic pH (Straubinger et al. 1990). A calibration curve of HPTS fluorescence emission as a function of pH was constructed as follows. 7 μM of HPTS solution was adjusted to various pHs and placed in a chamber slide with a focusing target. Images (exposure time = 0.1 and 0.3 s) were captured using a Zeiss CCD camera commanded by the Metamorph 3.0 software (Universal Imaging Corp., PA). The fluorescence intensity of calibration curves and HPTS-loaded umbrella cells was measured using the software Sigma Scan Pro 5.0 (Spss Inc. 1987–1999).

Immunofluorescence labeling

For tracing both endocytosed membrane-bound and fluid probes to the lysosomal compartment, the urothelial umbrella cells were labeled with the corresponding markers (IgG anti-UPIII and HPTS) followed by the induced endocytosis ("Fluid-probe endocytosis determination" and "Membrane-bound probe endocytosis determination" sections). Urothelium slides were obtained as described in "Fluid-probe endocytosis determination". For viewing the lysosomal compartment, in situ staining of a specific lysosome membrane protein was performed. The urothelial slides were previously fixed and washed with 1 % BSA and 5 % fat-free milk in PBS and finally incubated overnight at 4 °C with the primary antibody (mouse IgG anti-LAMP-1, 1:200, Santa Cruz Biotechnology) diluted in 1 % BSA–PBS. For negative controls, the incubation with the primary antibody anti-LAMP-1 was replaced with a non-relevant antibody (mouse IgG anti-nitric oxide sintase, Sigma Co). After primary antibody incubation, the slides were washed and incubated with an adequate rhodamine-conjugated secondary antibody (1:200, Sigma Co) for 2 h at 37 °C in the dark. Finally, the slides were washed with PBS and examined in a Carl Zeiss LSM5 Pascal laser scanning confocal microscope ("Fluid-probe endocytosis determination" section).

Colocalization of endocytotic markers and LAMP-1

The colocalization of endocytotic markers (HPTS and UPIII-FITC, green fluorescence) and lysosomal marker (anti-LAMP1, red fluorescence) was analyzed using the specific software ColocAna as described by Kreft et al. (2004). In summary, the percentage of colocalized pixels in each image relative to all green fluorescent pixels (total endocytosed marker) was assessed. The intensity value level of 51 AU, representing 20 % of the maximum intensity level, corresponds to the threshold value that separates the background intensity level from the signal.

Endocytotic probe recycling

Fluid-probe recycling

After the endocytosis of 20 mM DPX-solution (*p*-xylene-bis-pyridinium bromide, containing 22.2 mM glucose, 1.1

H_2KPO_4, 0.4 mM Na_2HPO_4, 5.4 mM KCl and 106 mM NaCl solution, pH 7.5, "Fluid-probe endocytosis determination" section), the urinary bladders were placed in cold PBS (to stop vesicle traffic). To remove the non-endocytosed fluid probe, the interior of the bladder was washed several times with cold PBS. Subsequently, the urinary bladders were filled with 200 µL of PBS and transferred to 37 °C to resume vesicle traffic. Subsequently, the luminal content of the urinary bladders was collected every 5 min and replaced each time with the same volume of PBS for a total of 50 min. The quantity of fluid probe (DPX) recycled in each aliquot was titrated with 1 µL of HPTS (7 µM). The HPTS fluorescence before (initial) and after (final) the addition to the recycled DPX was registered (SLM-Aminco spectrofluorometer) and the difference defined according to:

$$F_{initial} - F_{final} = \Delta F \quad (1)$$

where ΔF corresponded to the fluid probe recycled quantity in each aliquot. The ΔF values were expressed as percentage of the total endocytosed fluid probe ("Fluid-probe endocytosis determination" section). DPX endocytosis is stoichiometrically 1:1 in relation to HPTS (Grasso and Calderón 2009). Simultaneously, the same procedure was performed at 4 °C (no recycling condition) as negative control.

Membrane-bound probe recycling

In this case, the surface was labeled with IgG anti-UPIII, before endocytosis induction. To assay the probe recycling, we applied the same procedure to that of the fluid-probe recycling, but the recycled probe was collected in a PBS 0.5 % acetic acid solution and concentrated to 100 µL by lyophilization. The aliquots taken at different times were adjusted to pH of 7.4 and their fluorescence was expressed as percentage of the total endocytosed membrane-bound probe. Simultaneously, the same procedure was performed at 4 °C (no recycling condition) as negative control.

Protein determination

All protein determinations were according to Lowry et al. (1951).

Statistical analysis

All results are expressed as average of at least three independent experiments. Data obtained were statistically analyzed by ANOVA–Bonferroni tests and a level of less than $p < 0.05$ was chosen to detect significant differences using the statistical software InfoStat Professional version 1.1.

Results

Histological analysis

The histological analysis of urothelium slides derived from the dietary treatments and the classification of urothelial lesions was performed according to Cohen (2002). There were no inflammatory infiltrates, necrosis areas or hyperplastic, dysplastic and neoplastic lesions; thus, the urothelium derived from the dietary treatments was histologically compatible with normality (Fig. 1). Therefore, the alterations induced by the dietary treatments described in this work are not microscopically visible and are the results of modifications at the molecular and supramolecular levels.

Hydrophobic core structural parameters of urothelial endocytic vesicle membranes

In a previous work, we showed the fatty acid composition of different endocytic vesicle plasma membranes determined by gas chromatography (Grasso et al. 2011a) and

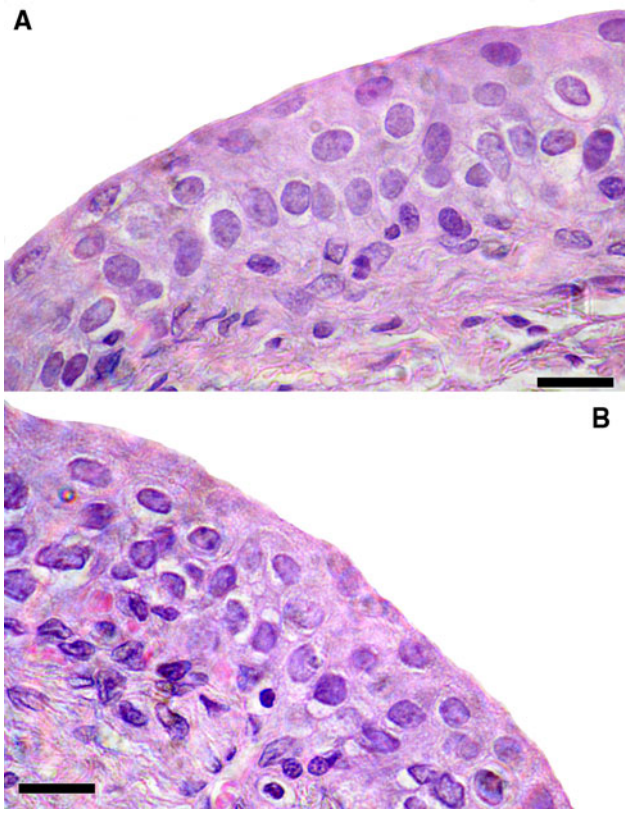

Fig. 1 Rat urothelium. HE-stained slides of rat urothelium derived from control diet (**a**) and oleic acid-enriched diet (**b**). The histological analysis on urothelium slides shows the absence of inflammatory infiltrates, necrosis or hyperplastic areas, or dysplastic or neoplastic lesions. All three diet-derived urothelium showed the same normality. *Scale bar* 10 µm

those values are reproduced in Table 1, second column. In OAV (oleic acid diet-derived vesicles), an increase in 16C–18C acyl chain-length concentration concomitant with a decrease in 20C–24C acyl chain-length concentration related to CV (control diet-derived vesicles) and LAV (linoleic acid diet-derived vesicles) (Grasso et al. 2011a) was observed. Those data were used to determinate the hydrophobic core structural parameters of urothelial endocytic vesicle membrane, applying the procedure reported by Mason et al. (1981). Calorimetric studies of those authors suggested that the effective chain length difference between the *sn-1* and *sn-2* acyl chains of phospholipids might affect the interdigitation of the fatty acyl chains across the bilayer center. Moreover, the depth of fatty acyl chains interdigitation determines the lipid-packing stability. Therefore, it was interesting to calculate, by taking into account the fatty acid composition of endocytic vesicle membranes (Grasso et al. 2011a) reproduced in Table 1, four average structural parameters: (1) the chain length (CL) of each fatty acid; (2) the "weighted" average chain length (WACL) of *sn-1* and *sn-2* acyl chains; (3) the effective inequivalence (interdigitation) or ΔC between *sn-1* and *sn-2* acyl chains and (4) the membrane-hydrophobic core thickness (HCT), Table 1. It was assumed in accordance with the natural phospholipid structure that: (1) the acyl chain bound to carbon atom 1 (*sn*-1 acyl chain) of the glycerol backbone is a saturated fatty acid, whereas that bound to carbon atom 2 (*sn*-2 acyl chain) is predominantly an unsaturated one; (2) there is random fatty acyl chain mixing in the phospholipids; (3) the chain length (CL, Table 1), expressed as C–C bonds, is equal to (n_1-1) and to (n_2-1-1.5-X) for saturated and unsaturated chains, respectively. n_1 and n_2 are the numbers of carbon atoms in the *sn*-1 and *sn*-2 acyl chains; 1.5 means the conformational shortening due to the abrupt bend at the C(2) atom of the *sn*-2 acyl chain and X is the effective average shortening of each double bond (0.5 times the number of double bonds of each fatty acid). We also determined the weighted average

Table 1 Average structural parameters of endocytic vesicle membrane with modified lipid composition

Fatty acids	CV			LAV		OAV	
	%	CL	WACL	%	WACL	%	WACL
Saturated							
14:0	3.84	13.00	0.50	5.61	0.73	2.85	0.37
16:0	28.54	15.00	4.57	29.75	4.76	46.64	7.46
18:0	39.89	17.00	6.78	28.77	4.89	40.14	6.82
20:0	0.00	19.00	0.00	0.65	0.12	0.00	0.00
22:0	0.00	21.00	0.00	0.00	0.00	1.58	0.33
24:0	29.00	23.00	6.67	35.22	8.10	8.79	2.02
Total	100.00		18.52	100.00	18.60	100.00	17.01
Unsaturated							
14:1	4.10	11.00	0.45	5.83	0.64	3.88	0.43
16:1	0.76	13.00	0.10	2.55	0.33	1.77	0.23
18:1 ω9	19.95	15.00	2.99	18.27	2.74	29.20	4.38
18:2 ω6	19.47	14.50	2.82	16.49	2.39	22.56	3.27
18:3 ω6	1.37	14.00	0.19	8.73	1.22	6.49	0.91
18:3 ω3	0.55	14.00	0.08	0.86	0.12	0.00	0.00
20:1 ω9	3.99	17.00	0.68	5.53	0.94	9.94	1.69
20:2 ω9	1.00	16.50	0.17	9.45	1.56	4.16	0.69
20:3 ω9	0.00	16.00	0.00	10.75	1.72	0.97	0.16
20:4 ω6	0.81	15.50	0.13	18.61	2.88	17.08	2.65
20:3 ω3	37.10	16.00	5.94	1.25	0.20	0.24	0.04
22:1 ω9	0.00	19.00	0.00	0.28	0.05	0.82	0.16
20:5 ω3	10.89	15.00	1.63	1.40	0.21	2.89	0.43
22:6 ω3	0.00	16.50	0.00	0.00	0.00	0.00	0.00
24:1	0.00	20.50	0.00	0.00	0.00	0.00	0.00
Total	100.00	100.00	15.17	100.00	15.01	100.00	15.02

	CV	LAV	OAV
ΔC	3.73 ± 0.24	3.6 ± 0.17	1.99 ± 0.22*
HCT	33.97 ± 0.33	33.61 ± 0.12	32.01 ± 0.22*

Fatty acid profile and structural parameters: *CL* acyl chain length, *WACL* weighted average chain length, *ΔC* acyl chain interdigitation, *HCT* membrane-hydrophobic core thickness. CV, LAV and OAV mean control vesicles, linoleic acid-derived and oleic acid-derived vesicles, respectively

* Significant statistical difference ($p < 0.05$, ANOVA–Bonferroni test)

chain length of *sn*-1 and *sn*-2 fatty acid (WACL = % of each FA. CL/100). ΔC is the effective inequivalence (in C–C bonds) between the two, saturated and unsaturated acyl chains, corresponding to the difference between $WACL_{sat}$ and $WACL_{unsat}$ (Table 1). According to Wang et al. (1995), the hydrophobic core thickness corresponds to the sum of the saturated and unsaturated WACLs. The results showed the lower interdigitation (ΔC) of the acyl chains in OAV related to CV (1.99 ± 0.22 vs. 3.73 ± 0.24, respectively). Concomitantly, a small but significant decrease in the hydrophobic core thickness in OAV compared to CV was observed (32.01 ± 0.22 vs. 33.97 ± 0.33, respectively). We did not observe significant differences between CV and LAV. Finally, with the purpose of illustrating with a simplified model the possible conformation of the phospholipid acyl chains, the ΔC and HCT parameters were proportionally combined and interpreted on the basis of molecular packing (Fig. 2).

Fluid-probe endocytosis

Fluid-probe (HPTS) endocytosis by the umbrella cells was induced for 20 and 40 min, as described in "Fluid-probe endocytosis determination". The quantity of endocytosed material (fluorescence) was measured by spectrofluorometric assays and by confocal microscopy. Before measuring, the pH of the samples was adjusted to 7.3 to neutralize the pH effect on the probe (see "Fluid-probe endocytosis determination"). We observed by spectrofluorometric assays that the amount of endocytosed material (8.35 ± 0.3 and 8.1 ± 0.2 % after 20 and 40 min of endocytosis induction, respectively) by umbrella cells derived from oleic acid-enriched diet was lower than that of the control umbrella cells (12.13 ± 0.42 and 12.7 ± 0.22 %; Fig. 3a). In parallel, we measured the fluorescence intensity in umbrella cell images (captured by confocal microscopy) using the Sigma Scan Pro software, calibrated to express the total fluorescence intensity per μm^2 of urothelium (the measurements were performed on approximately 53,000 μm^2 of urothelium corresponding to at least 30 images). We confirmed by this methodology the lower endocytosis of umbrella cells derived from oleic acid-enriched diet at both times of endocytosis induction (48.4 ± 2.8 and 51.8 ± 3.08 AU, at 20 and 40 min of endocytosis induction, respectively) compared to control umbrella cells (71.95 ± 3.8 and 66.7 ± 3.3 AU; Fig. 3b). The difference between linoleic acid-enriched diet-derived cells and control umbrella cells was not significant.

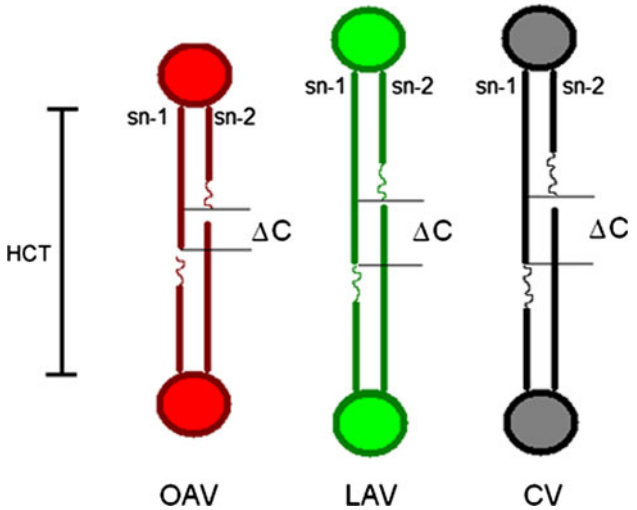

Fig. 2 Diagram illustrating the possible association of phospholipids fatty acids from endocytic vesicle membranes. *ΔC* acyl chain interdigitation, *HCT* hydrophobic core thickness. sn-1 and sn-2 correspond to saturated and unsaturated fatty acid position in the phospholipid molecule, respectively. The "wavy" segments represent the unsaturated segment lengths of the fatty acyl chains. All values are proportionally represented

Membrane-bound probe endocytosis

We induced the membrane-bound probe (IgG anti-UPIII) endocytosis by the umbrella cells for 20 and 40 min, as described in "Membrane-bound probe endocytosis determination". After the induction of endocytosis, the spectrofluorometric assays indicated that umbrella cells derived from oleic acid-enriched diet also endocytosed less membrane-bound probe (5.42 ± 0.32 and 5.22 ± 0.11 % at 20 and 40 min of endocytosis induction, respectively) compared to control umbrella cells (16.43 ± 0.95 and 15.81 ± 0.34 %; Fig. 3c). The pH effect on the fluorescence was discounted by adjusting the pH of the membrane suspension to 7.4, before each measurement. The results were confirmed by analyzing the umbrella cell images captured by confocal microscopy. The microscopy assays showed the lower endocytosis of membrane marker by umbrella cells derived from oleic acid-enriched diet at both times of endocytosis induction (53.7 ± 4.5 and 52.05 ± 3.04 AU at 20 and 40 min of endocytosis induction, respectively) compared to control umbrella cells (77.76 ± 4.92 and 83.01 ± 5.65 AU; Fig. 3d). No significant difference between linoleic acid-enriched diet-derived umbrella cells and control umbrella cells was observed.

Endocytic vesicle pH measurements

We determined the luminal pH of HPTS-loaded urothelial endocytic vesicles, differentiated in their lipid composition by spectrofluorometric assays and epifluorescence microscopy. The pH dependence of HPTS fluorescence emission is the result of reversible proton dissociation from the hydroxyl group on the trisulfonated pyrene ring.

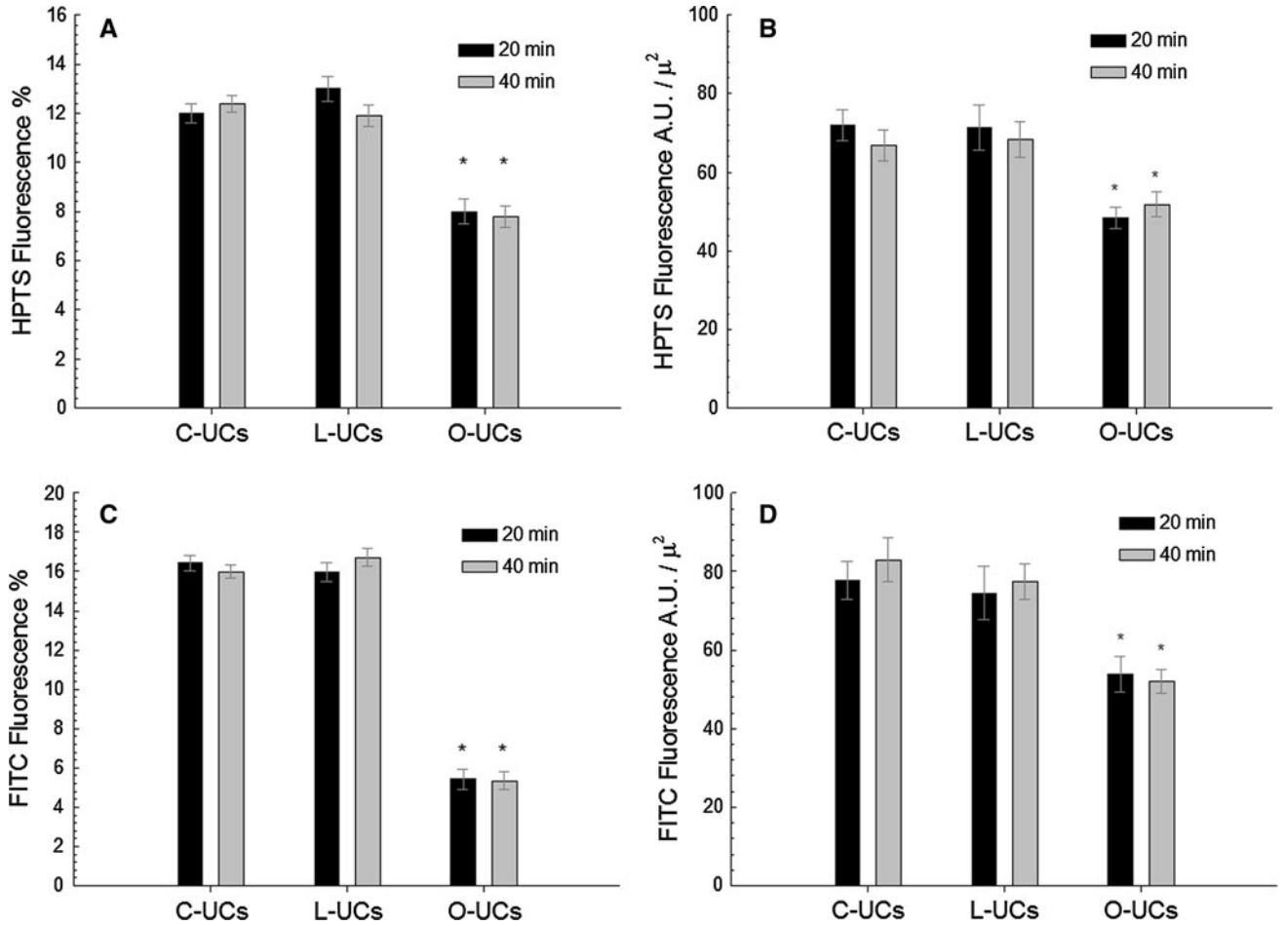

Fig. 3 Measurements of endocytotic capacity. Fluid-probe endocytosis. **a** The fluorescence values were determined spectrofluorometrically and expressed as a percentage of the total luminal probe. C-UCs, L-UCS and O-UCs mean control umbrella cells, umbrella cells derived from linoleic acid-enriched diet and oleic acid-enriched diet, respectively. 20 and 40 min correspond to the elapsed time of endocytosis induction. O-UCs endocytosed the lesser amount of fluid probe at both times. **b** The values were expressed as total fluorescence per μm^2 of urothelium (the measurements were performed on approximately 53,000 μm^2 of urothelium, corresponding to at least 30 images, captured by confocal microscopy). The data correlate with the fluorescence assays, shown in **a**. **c**–**d** Membrane-bound probe endocytosis. The values are expressed as described in **a**–**b**. O-UCs also endocytosed the lesser amount of membrane-bound probe. *Significant statistical difference ($p < 0.05$, ANOVA–Bonferroni test)

Fluorescence increases with pH at λ_{exc} 470 nm and decreases at λ_{exc} 405 nm Fig. 4a; (Straubinger et al. 1990). Fluorescence ratios at λ_{exc}405 nm/λ_{exc}470 nm were used for reporting physiological pH (4.5–7.4). The fluorescence of HPTS solutions prepared at different pH were measured by spectrofluorometry and epifluorescence microscopy and used to construct the respective calibration curves of emission intensity ratios as a function of pH (Fig. 4b). For the spectrofluorometric assays, the endocytic vesicles were isolated and the fluorescence emitted at λ_{exc} 405 nm and λ_{exc} 470 nm was measured and converted to pH values. We observed a higher pH value in OAV (6.36 ± 0.05) in relation to CV and LAV (5.72 ± 0.03 and 5.74 ± 0.04, respectively; Fig. 5). The lower acidification observed in OAV correlates with the lower proton translocation of V-ATPase in OAV, as previously reported (Grasso et al. 2011a).

In parallel, we measured the endocytic vesicle pH by epifluorescence microscopy. To this purpose, umbrella cells derived from the dietary treatments were loaded with HPTS by endocytosis induction during 20 and 40 min (see "Endocytic vesicles pH measurements"; Fig. 6a). This procedure allows following the acidification progress. Unlike spectrofluorometric assays, the epifluorescence microscopy allowed us to determine the pH of intracellular vesicles without their previous isolation (Fig. 6b). We observed a higher average pH value of the OAV after 20 and 40 min of endocytosis induction (6.26 ± 0.05 vs. 5.82 ± 0.07 of control vesicles after 20 min and 5.75 ± 0.06 vs. 5.6 ± 0.04 of control vesicles after 40 min). There

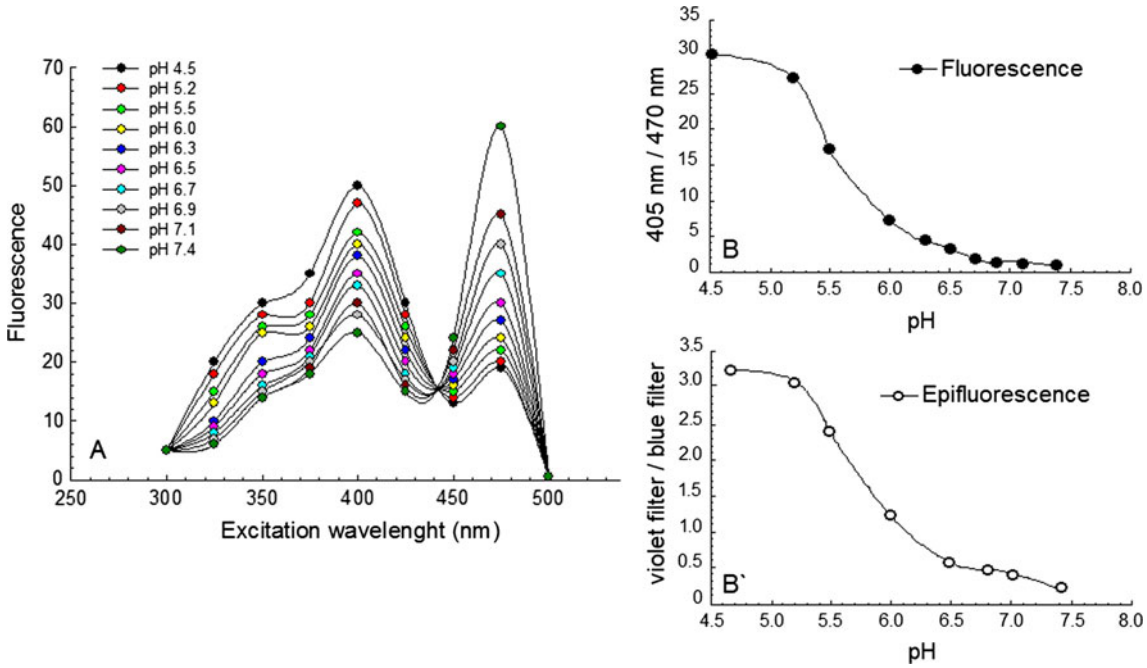

Fig. 4 **a** Excitation spectra of HPTS in the pH range of 4.5–8.0. HPTS 7 μM in PBS was adjusted to various pH, and the excitation wavelength (λ_{exc}) was scanned over the range of 300–500 nm. Fluorescence emission was detected at 510 ± 5 nm at the following pH: 7.4, 7.1, 6.9, 6.7, 6.5, 6.3, 6.0, 5.5, 5.2 and 4.5. The pH 7.4 *curve* can be identified as that with the highest intensity at 470 nm and the lowest intensity at 405 nm. **b** pH calibration curves for HPTS. Fluorescence (**b**) and epifluorescence (**b′**) microscopy determination. Fluorescence emission was measured at the λ_{exc} 405 and 470 nm and expressed as the emission ratio at both λ_{exc}. In the case of epifluorescence, the values are expressed as the emission ratio at both excitation filters, violet (λ_{exc} 365–412 nm) and blue (λ_{exc} 450–490 nm)

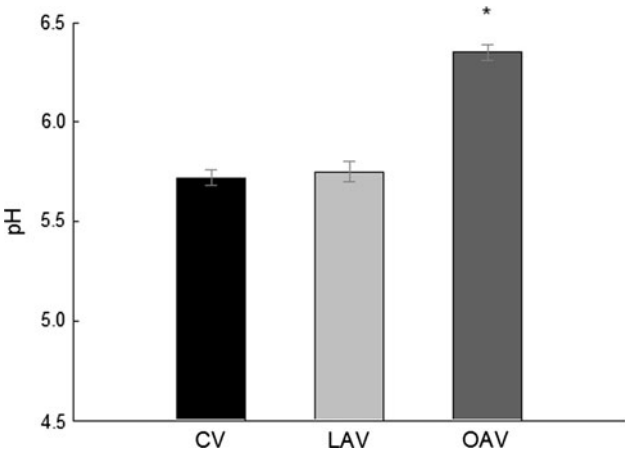

Fig. 5 Spectrofluorometric determination of vesicles' pH. Endocytotic vesicles were isolated as described ("Endocytic vesicles pH measurements" section) and the luminal pH values were determined using the calibration curve and the emission ratio at λ_{exc} 405 and 470 nm as described in "Endocytic vesicles pH measurements". OAV showed the highest pH value. *Significant statistical difference ($p < 0.05$, ANOVA–Bonferroni test)

were no significant pH differences between the values of CV and LAV. However, in all types of vesicles, the pH decreases as a function of time probably indicating the progression of the endocytosed material to the lysosome.

Colocalization of endocytotic probes in the lysosomal compartment

Fluid probe

The urothelial endocytic vesicles were loaded with HPTS by endocytosis induction for 20 and 40 min (see "Fluid-probe endocytosis determination"). Cryosections of urothelium obtained as indicated in "Fluid-probe endocytosis determination" were fixed and immunostained with lysosome membrane-specific antibody (LAMP-1) and revealed with a rhodamine-conjugated secondary antibody (see "Immunofluorescence labeling"). The HPTS fluorescence was viewed with a confocal microscope equipped with a multiline argon laser (λ_{exc} 458, 488 nm and λ_{em} 514 nm). The rhodamine fluorescence, corresponding to the lysosome membrane, was viewed using two helium–neon lasers (λ_{exc} 543 nm and λ_{em} 633 nm; Fig. 7a). Captured images were analyzed with the custom ColocAna software specific for confocal colocalization analysis (Kreft et al. 2004). This software defines the colocalization coefficient as the pixels emitting signal in both channels (red and green) related to the pixels emitting signal in the green channel (total endocytosed probe).In the urothelium derived from the three dietary treatments, we observed a

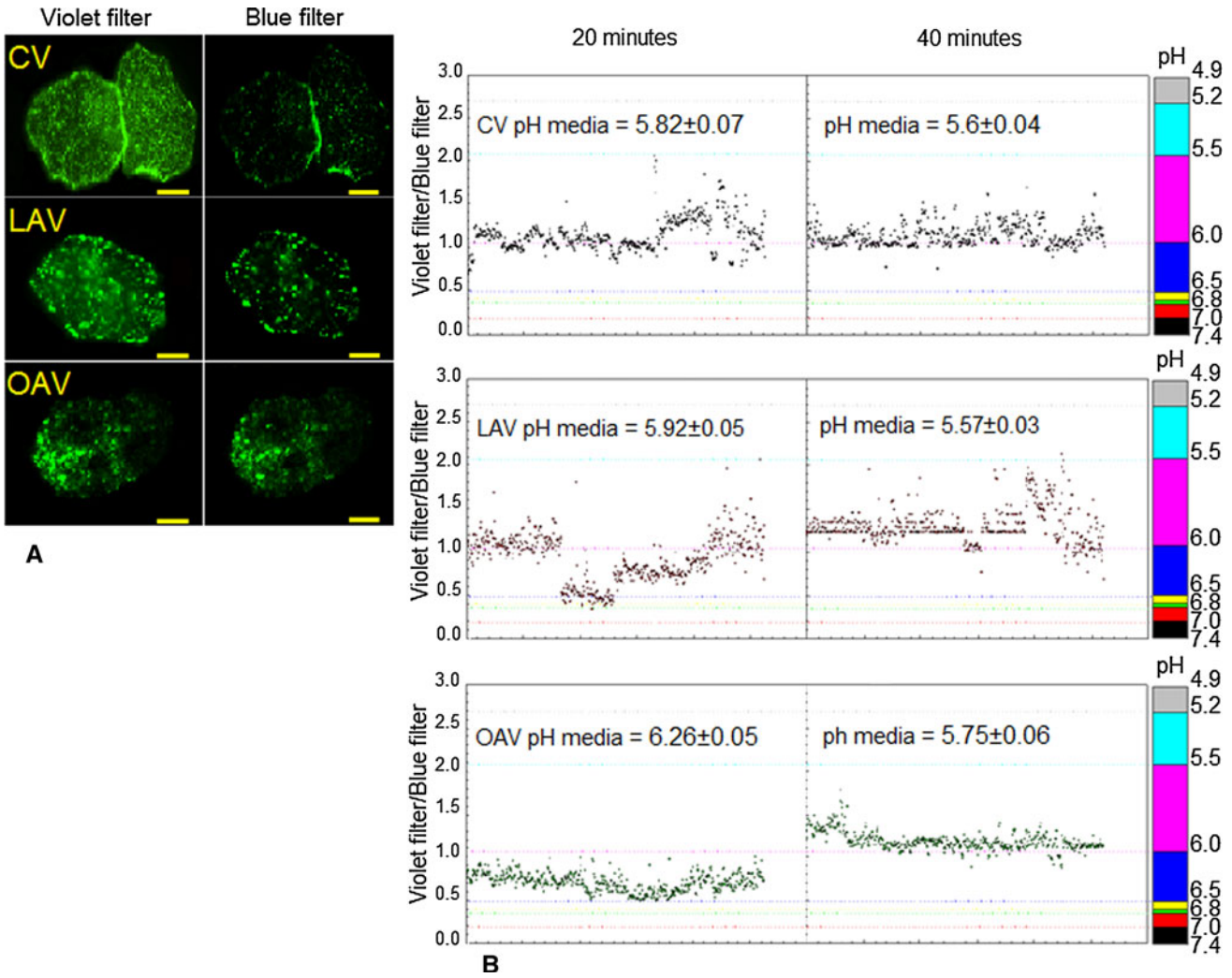

Fig. 6 **a** Epifluorescence pH determination of umbrella cells loaded with HPTS. **a** The fluorescence intensity of HPTS-loaded umbrella cells was determined by using a violet filter (λ_{exc} 365–412 nm) and a blue filter (λ_{exc} 450–490 nm). The images were captured with a CCD camera and analyzed with the Sigma Scan Pro software. The fluorescence intensity decrease, in *right panels* (*blue filter*), indicates the probe acidification. *Scale bar* 10 μm. **b** The pH of umbrella cells' endocytic vesicles loaded with HPTS (*scale bar*) was calculated by using the emission ratio of the image sets (*violet filter/blue filter*) and the calibration curve (Fig. 4, B′). The pH of at least 1,000 vesicles of each dietary treatment at two times of endocytosis induction (20 and 40 min) was determined. OAV showed the highest pH values of intracellular vesicles at both times of endocytosis induction. Nevertheless, the pH of the endocytic vesicles decreased as a function of time in all the cases

relative increase, as a function of time, of HPTS-loaded endocytic vesicle colocalization with lysosome. Surprisingly, OAV showed lower colocalization coefficients at both times of endocytosis (0.05 ± 0.008 and 0.14 ± 0.008 after 20 and 40 min, respectively) versus CV coefficients (0.09 ± 0.01 and 0.18 ± 0.01) and LAV coefficients (0.08 ± 0.01 and 0.18 ± 0.012; Fig. 7b).

Membrane-bound probe

We performed a similar procedure, as described for the fluid-probe colocalization analysis, but the endocytosed probe was the IgG anti-UPIII attached to the urothelial plaques of umbrella cells (see "Membrane-bound probe endocytosis determination"). After endocytosis induction, urothelium cryosections were obtained and stained with IgG anti-LAMP-1 (Fig. 8a). Images of the cryosections were captured and analyzed as described for the fluid-probe colocalization analysis. Similarly to that observed for fluid probe, the colocalization coefficients were increased as a function of time in all types of endocytic vesicles. However, OAV also showed lower colocalization coefficients at both times of endocytosis (0.25 ± 0.04 and 0.47 ± 0.07 after 20 and 40 min, respectively) compared to CV coefficients (0.45 ± 0.05 and 0.65 ± 0.09) and LAV coefficients (0.39 ± 0.04 and 0.61 ± 0.05; Fig. 8b).

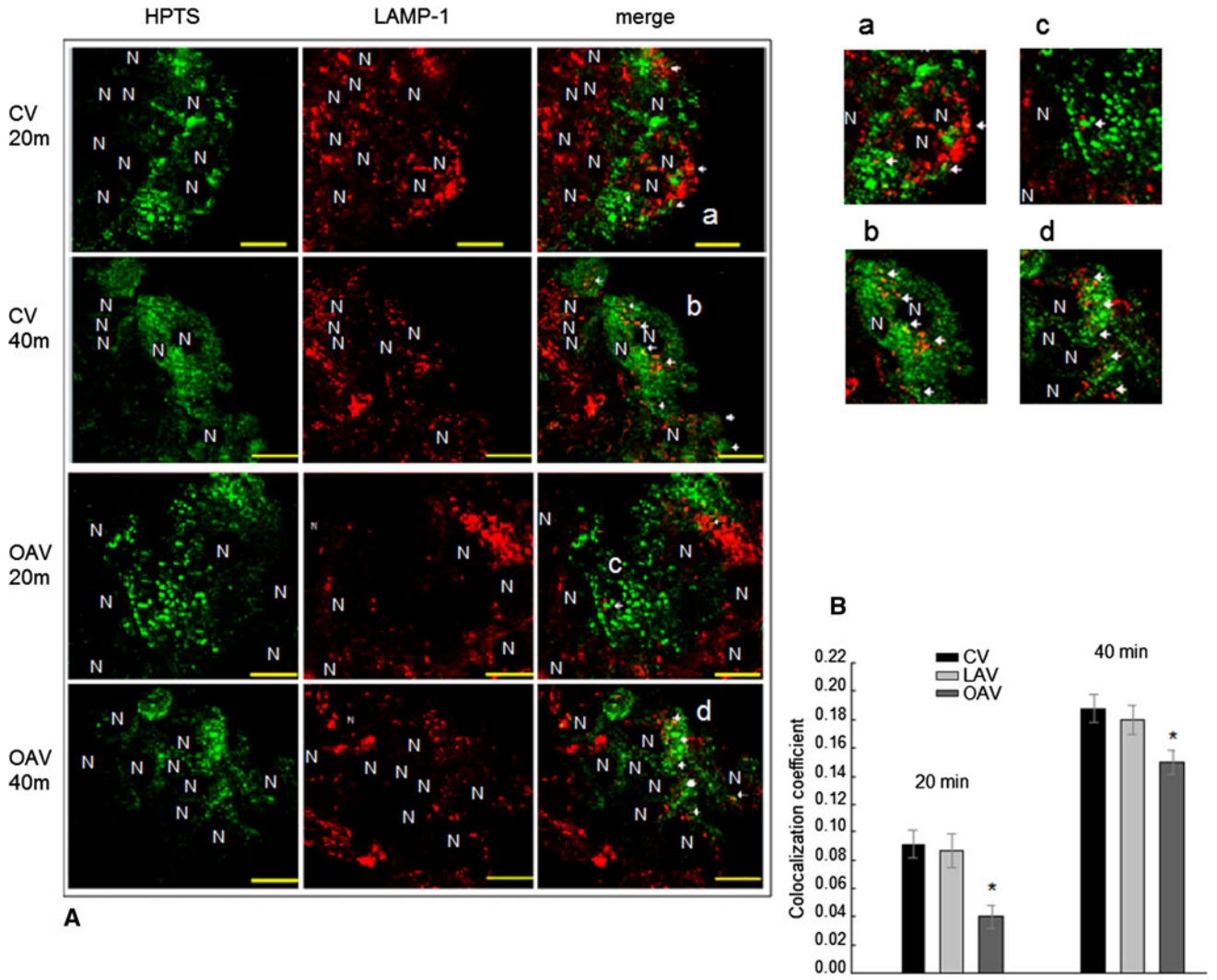

Fig. 7 **a** Colocalization of the endocytosed fluid probe and the lysosome-specific probe in the lysosomal compartment. *Left panels* (*green*): cryosections of umbrella cells loaded with HPTS by endocytosis induction for 20 and 40 min. *Central panels* (*red*): umbrella cells immunostained with the anti-lysosome membrane protein (LAMP-1) antibody. *Right panels* (*merge*): the colocalization of the probes was observed by overlapping the right and central panels with Adobe Photoshop. *a*, *b*, *c* and *d*: digital magnification corresponding to colocalized representative zones. No differences were observed between CV and LAV. *N* nuclei, *arrows* colocalized structures. *Scale bar* 10 µm. **b** Colocalization coefficients of fluid probe and lysosome. The coefficients were determined by the ColocAna software. OAV showed the lowest coefficient at both times of endocytosis induction. *Significant statistical difference ($p < 0.05$, ANOVA–Bonferroni test)

Fluid-probe recycling

DPX endocytosis was induced as described in "Fluid-probe endocytosis determination". Subsequently, the recycled DPX was collected by successive washing of the bladder′s luminal cavity every 5 min. The DPX content of the aliquots was titrated with HPTS. The fluorescence decrease in the added HPTS indicated the return (recycling) of the quencher DPX to the luminal cavity. All values were expressed as the difference in HPTS fluorescence before (initial) and after (final) being added to the recycled DPX, according to Eq. (1) ("Endocytotic probe recycling" section), and finally normalized as percentage of total DPX endocytosed. As indicated in Fig. 9a, OAV and LAV showed higher fluid-probe recycling than CV. The total recycled material (defined as the sum of all collected aliquots every 5 min) determined for OAV and LAV was 8.39 ± 0.32 % and 6.42 ± 0.21, respectively. CV showed lower recycling value: 2.85 ± 0.18 %. As negative control (no recycling), we performed simultaneously the same experimental procedure keeping the temperature constant at 4 °C throughout the experiment to stop all the vesicular traffic.

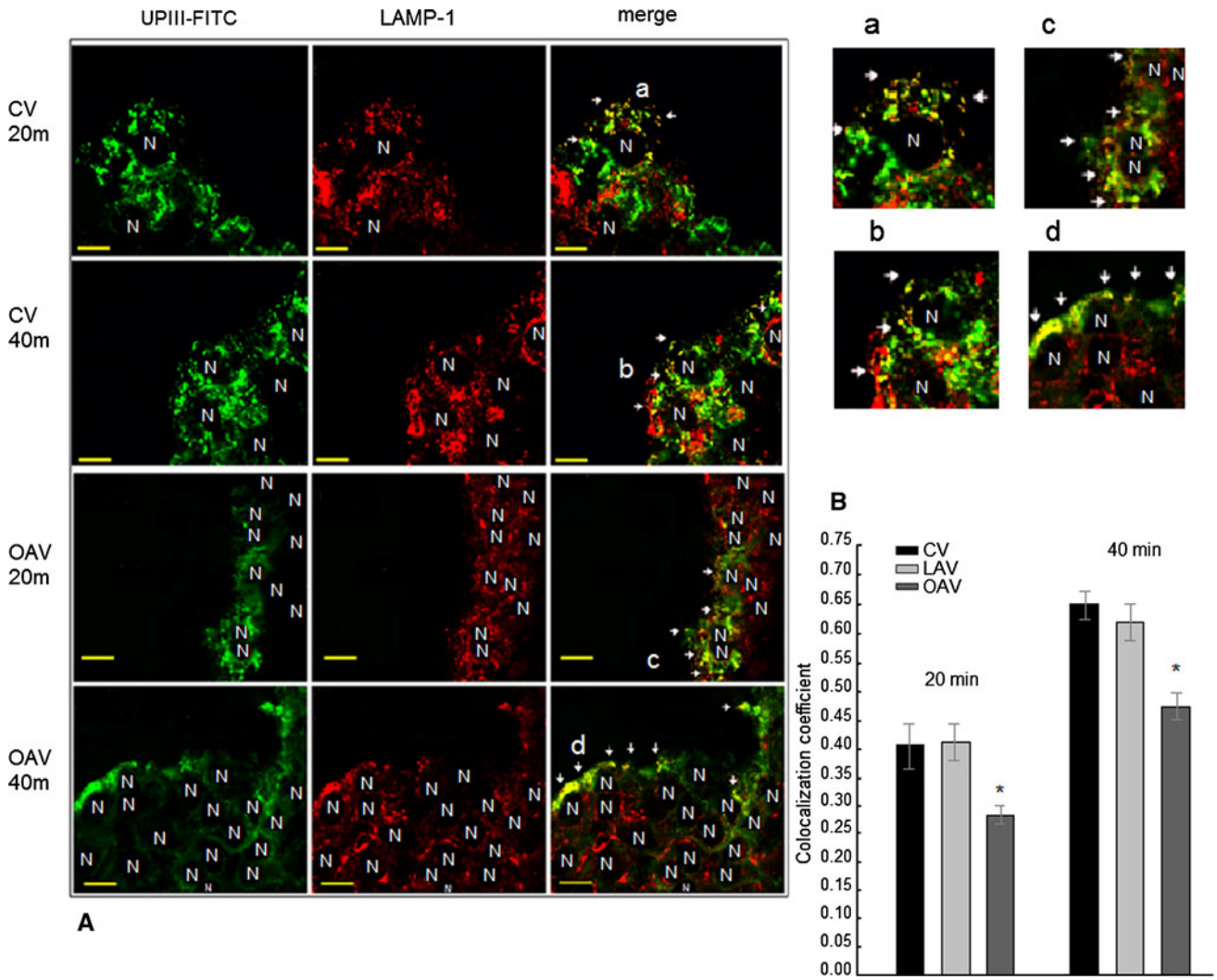

Fig. 8 **a** Colocalization of the endocytosed membrane-bound probe and the lysosome-specific probe in the lysosomal compartment. *Left panels* (*green*): cryosections of umbrella cells showing the internalized probe (UPIII-FITC). *Central panels* (*red*): umbrella cells immunostained with the anti-lysosome membrane protein (LAMP-1) antibody. *Right panels* (*merge*): the colocalization of the probes was observed by overlapping the right and central panels with Adobe Photoshop. *a*, *b*, *c* and *d*: digital magnification corresponding to colocalized representative zones. *a*, *b*, *c* and *d*: digital magnification corresponding to colocalized representative zones. No differences were observed between CV and LAV. *N* nuclei, *arrows* colocalized structures. *Scale bar* 10 μm. **b** Colocalization coefficients of membrane-bound probe and lysosome. OAV showed the lowest coefficient at both times of endocytosis induction. *Significant statistical difference ($p < 0.05$, ANOVA–Bonferroni test)

Membrane-bound probe recycling

With the purpose of studying the recycling of the membrane-bound probe, we induced endocytosis of the surface membrane immunostained with a specific antibody against the urothelial plaques as described in "Membrane-bound probe endocytosis determination". The recycled material was collected by successive washing every 5 min during 50 min ("Endocytotic probe recycling" section). The fluorescence intensity of collected aliquots was expressed as percentage of the total fluorescence endocytosed. Figure 9b indicates the higher recycling of membrane-bound probe in OAV (26.45 ± 3.67 %) versus CV (7.12 ± 2.78 %). We did not observe significant differences between CV and LAV. As negative control (no recycling) ,we performed simultaneously the same experimental procedure, keeping the temperature constant at 4 °C throughout the experiment to stop all vesicular traffic.

Fractional distribution of endocytosed material in the different intracellular compartments

We calculated the fractional distribution of the endocytosed material in the two endocytotic pathways described in this paper (recycling and lysosomal degradation) and the cytosolic leakage previously reported (Grasso and

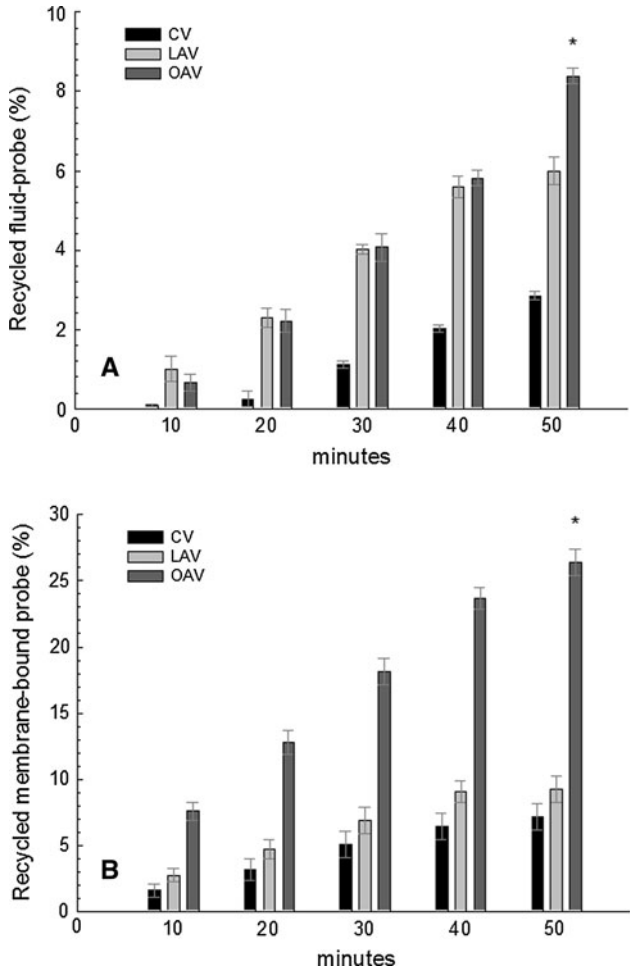

Fig. 9 Recycling of the endocytosed probes. The fluid probe (**a**) and membrane-bound probe (**b**) were measured after the exocytosis at the urinary bladder lumen. In **a** each value represents the sum of all ΔF (see "Endocytotic probe recycling") preceding that at the indicated time. In B, each value represents the sum of the proceeding values at that time. All values are expressed as percentage of the recycled probe related to the inoculated total probe. The highest recycling values of either fluid or membrane-bound probes were observed in OAV. As negative control (for both probes), the same procedure was performed at 4 °C. All values correspond to the average of three independent determinations ± SEM. *Significant statistical difference ($p < 0.05$, ANOVA–Bonferroni test)

Calderón 2009). The total endocytosed material (fluid and membrane-bound probes), released by the respective cell suspension after the addition of Triton X-100, was taken as 1. Thus, all values corresponding to each pathway were converted to fractions of 1. The results are shown in Table 2. As the sum of all fractions did not reach unity, the remaining quantity could be located in the endosomes (Romih and Jezernik 1994).We observed that the colocalization of endocytosed fluid probe and lysosome marker at 40 min of endocytosis induction was lower in OAV (0.14 ± 0.01) compared to CV and LAV (0.18 ± 0.012 and 0.182 ± 0.01, respectively). On the contrary, OAV

Table 2 Fractional distribution of endocytosed probes

	CV	LAV	OAV
Fluid-probe			
Endocytosis	1	1	1
Endosomes	0.49 ± 0.031	0.47 ± 0.045	0.35 ± 0.032*
Recycling	0.02 ± 0.001	0.06 ± 0.014*	0.08 ± 0.011*
Leakage	0.29 ± 0.035	0.28 ± 0.021	0.42 ± 0.04*
Lysosome	0.18 ± 0.012	0.18 ± 0.012	0.14 ± 0.01*
Membrane-bound probe			
Endocytosis	1	1	1
Endosomes	0.27 ± 0.04	0.31 ± 0.02	0.33 ± 0.03
Recycling	0.07 ± 0.02	0.09 ± 0.03	0.26 ± 0.03*
Leakage	ND	ND	ND
Lysosome	0.65 ± 0.02	0.60 ± 0.04	0.41 ± 0.03*

The values of each determination were converted to fractions of the total endocytosed probe, as described in "Fractional distribution of endocytosed material in the different intracellular compartments". *ND* not determined. All values correspond to the average of three independent determinations ± SEM

* Significant statistical difference ($p < 0.05$, ANOVA–Bonferroni test)

recycled fluid probe to a greater extent (0.08 ± 0.011) than CV (0.02 ± 0.001). However, the main differences observed in OAV were the high fraction of leakage into the cytosol (0.42 ± 0.04) and the lower fraction remaining in the endosomes (0.35 ± 0.032).

The intracellular distribution of membrane-bound endocytosed probe changed substantially with respect to fluid-probe distribution. In this case, the probe cannot leak to the cytosol (due to stable union of probe to the membrane). The lysosomal colocalization in OAV at 40 min of endocytosis was lower (0.41 ± 0.03) compared to CV and LAV (0.65 ± 0.02 and 0.60 ± 0.04, respectively). Nevertheless, all vesicles showed a higher colocalization of the membrane-bound probe and the lysosomal probe compared to the fluid probe. The recycled fraction was also higher in OAV (0.26 ± 0.03) than CV and LAV (0.07 ± 0.02 and 0.09 ± 0.03, respectively).

"Weighted" average effect of endocytosis and acidification on the intracellular distribution of endocytic vesicles

Keeping in mind that the intracellular distribution of endocytosed material depends on complex interactions between different traffic pathways, regulated at molecular levels, we proposed a first approach to evaluate our results in terms of "weighted" average effect of each pathway on the intracellular fractional distribution of the endocytosed material. The "weighted" average effect (WAE) of each pathway was determined by the following equation:

$$WAE_x = (f_{Rec} \cdot f_x) + (f_{Endos} \cdot f_x) + (f_{Leak} \cdot f_x) + (f_{Lyso} \cdot f_x) \quad (2)$$

where f_{Rec} = fraction recycled; f_{Endos} = fraction at the endosomes; f_{Leak} = fraction released to the cytosol (leakage); f_{Lyso} = fraction at the lysosome; f_x = fraction of the considered parameter.

The results in Table 3 indicate that on comparing the WAE of each fluid pathway with the respective values of CV, the lower proton translocation activity (acidification) of the V-ATPase that we determined previously(Grasso et al. 2011a) showed the highest WAE (2.58 vs. 1.5, 0.38, 0.69 and 1.35 for endocytosis, recycling, leakage and lysosome, respectively).

On the other hand, by carrying out the same comparative analysis, but on membrane-bound probe, the highest WAE corresponded to the almost similar values of endocytotic capacity and the V-ATPase activity (3.0 and 2.75 vs. 0.27 and 1.59 for recycling and lysosome, respectively).

Discussion

Vesicular trafficking is an essential cellular process in eukaryotic cells to deliver either membrane proteins or soluble cargos from one compartment to another (Marshansky and Futai 2008). It has been shown that the intracellular traffic can be regulated, among others, by the luminal acidic pH of intracellular organelles established by a transmembrane pH gradient and/or membrane potential (Marshansky and Futai 2008). On the other hand, it was recently demonstrated that the endocytotic traffic in umbrella cells was not regulated either by clathrin or caveolin; instead, it is regulated by integrin, dynamin and RhoA (Khandelwal et al. 2010). Other authors had demonstrated that endocytotic capacity was also regulated by the differentiation stage of umbrella cells (Kreft et al. 2009). Nevertheless, how the membrane lipid composition and its derived structural organization can affect cellular traffic has not yet been studied. Thus, the results reported in this work are, to our knowledge, the first approach to understand how the vesicular acidification rate is modulated by the membrane lipid composition and, consequently affect the particular fate of the urothelial vesicles.

In trying to understand our results, we may consider intracellular traffic as a dynamic equilibrium between the influx (endocytosis) and efflux (exocytosis) of materials governed mainly by the acidification of an early endocytic/endosomal compartment. Our results seem to correlate with this statement. In fact, the lower endocytosis observed in umbrella cells derived from oleic acid-enriched diet (Fig. 3) was concomitant with the lower acidification rate reported for the oleic acid-derived vesicles (OAV) compared to linoleic acid-derived vesicles (LAV) and control vesicles (CV) (Grasso et al. 2011a). This suggested that the lower activity of the V-ATPase in OAV was due to the uncoupling of the V-ATPase domains (Grasso et al. 2011a). To further explore how membrane lipids can affect vesicle membrane proteins in such a way as to alter the V-ATPase functionality, we now calculated, from the fatty acid analysis (shown in Table 1), some average structural parameters: acyl chain length (CL), weighted average chain length (WACL), acyl chain interdigitation (ΔC) and membrane-hydrophobic core thickness (HCT). As shown in Table 1, both acyl interdigitation and hydrophobic core thickness are lower in OAV compared to CV and LAV. This may imply some lipid matrix alterations, leading to a lipid–protein hydrophobic mismatch (Lee 2004). It was proposed that the exposure of the enzyme hydrophobic fragments to the aqueous phase could induce the stretching of surrounding fatty acyl chains favored by the lower interdigitation (Lee 2004). Whatever the hydrophobic mismatch could be, it represents an alteration of the lipid matrix surrounding the enzyme. This condition could be reflected in the altered capacity of the proton-transporter domain (V_0) to function in phase with the catalytic domain (V_1) and consequently lead to a modified acidification rate of the V-ATPase in OAV, as previously reported (Grasso

Table 3 "Weighted" average effect of endocytosis and acidification on the intracellular distribution of endocytic vesicles

Probes	WAE				
	Endocytosis	V-ATPase	Recycling	Leakage	Lysosome
Fluid					
CV	0.12	0.31	0.03	0.29	0.19
LAV	0.13	0.33	0.06	0.28	0.18
OAV	0.08	0.12	0.08	0.42	0.14
CV/OAV	1.50	2.58	0.38	0.69	1.35
CV/LAV	0.92	1.00	0.50	1.04	1.06
Membrane bound					
CV	0.16	0.31	0.07	–	0.65
LAV	0.15	0.33	0.09	–	0.60
OAV	0.05	0.12	0.26	–	0.41
CV/OAV	3.00	2.75	0.27	–	1.59
CV/LAV	1.07	1.00	0.78	–	1.08

The "weighted" average effect (WAE) of each pathway corresponds to the sum of the products of the respective fractions (Table 2) by the fraction of the considered parameter ("Weighted" average effect of endocytosis and acidification on the intracellular distribution of endocytic vesicles section). To determine the WAE of V-ATPase and leakage, the corresponding values were taken from Grasso et al. 2011a and Grasso and Calderón 2009, respectively

et al. 2011a). Taking into account these results and making a correlation with the lesser thickness of the OAV-hydrophobic core conformation (Fig. 2) found in this work, we suggest that the lipid matrix alterations inducing a modified acidification rate of the endocytosed vesicles could modulate the delivery of the endocytosed cargo to the lysosomal compartment (Figs. 7, 8). This was corroborated by analyzing the colocalization of both fluid and membrane-bound probes with a lysosomal marker. The lower colocalization in OAV (Figs. 7, 8) was related to lower vesicle acidification (Figs. 5, 6).

On the other hand, how can the endocytosis be regulated by membrane lipid composition/vesicle acidification? We must consider previous results related to membrane organization. The association of oleic acid and PE (phosphatidylethanolamine) induces the formation of inverted tubular micelles, which are the basic supramolecular units of H_{II} (inverted hexagonal) arrays (Wasungu et al. 2006). Coincident with that result, we observed an increased oleic acid concentration (Calderón and Eynard 2000; Grasso et al. 2011a) as well as an increased amount of PE in oleic acid-derived urothelial membranes (Bongiovanni et al. 2005) compared to control and linoleic acid-derived membranes. Simultaneous to those changes, an altered structural organization of urothelial plaques derived from the oleic acid-enriched diet was found after morphometric analysis of negatively stained electron microscopy images (Calderón and Grasso 2006). In addition, we reported that, although the average molecular rigidity of oleic acid-derived urothelial membranes is lower than that of the control and linoleic acid-derived membranes, an increased rigidity in the half of the hemilayer was determined in oleic acid-derived membranes (Calderón and Eynard 2000), when analyzing the degree of freedom along the acyl chain depth (Baenziger et al. 1991). Moreover, an increased membrane saturation degree, which is associated with a diminished endocytosis in mouse peritoneal macrophages (Mahoney et al. 1997), was also observed in OAV (Fig. 3). Thus, the lipid composition, mainly lipid organization, membrane rigidity and membrane saturation degree, are all parameters related to membrane structure, as demonstrated in synthetic lipid systems (Nagle and Tristam-Nagle 2000; Funari et al. 2003). All of these parameters, differentially altered in OAV, appear concomitant with the lower endocytosis processes. These results are in agreement with the results of Truschel et al. (2002). They reported that mechanical stretch induced the maximum endocytosis as early as 5 min, and this value did not change up to 120 min even if exocytosis may occur simultaneously. Furthermore, those authors demonstrated that the membrane capacitance changes, as a function of time, showed a biphasic tracing with faster changes up to 20 min followed by a remarkably slow trend from 40 to 300 min, both trends isolated by constant values between 20 and 40 min. Indeed, an equilibrium between endocytosis/exocytosis was reached at 20–40 min (Fig. 3). In conclusion, our results suggest that the vesicle acidification (V-ATPase activity) and endocytosis processes were both dependent on membrane lipid composition in our OAV.

Membrane recycling is a necessary event after any endocytosis processes (Perez Bay et al. 2011). In fact, the model of urothelial endocytic vesicle traffic, proposed by Hicks, defined the endocytic/exocytic events as the response to changes in hydrostatic pressure during the micturition cycle (Hicks 1975). Nevertheless, in trying to understand how lipid composition and/or vesicle acidification may modulate the vesicle traffic pathways, we also studied the recycling processes in our three diet-derived vesicles. The results in Fig. 9 show that the material recycled throughout 50 min after endocytosis was higher in OAV when compared with CV and LAV, while in this particular vesicle type the endocytosed material delivered to lysosome was lower. These results also correlated with the "weighted" average effect, shown in Table 3, where the WAE of the recycling increased (WAE < 1) concomitantly with the decrease of both V-ATPase activity and lysosomal WAE (>1) (Table 3). This probably reflected once again how the lipid membrane composition, inducing the uncoupled V-ATPase activity, plays a critical role, indicated by the highest "weight" of its dysfunction (2.58) on the fractional distribution of the studied pathways (Table 3). These results might be considered as a displacement to recycling of vesicles targeted for degradation in order to keep the balance between endocytosis/exocytosis. We suggest that, even if the amount of endocytosed material is lower in OAV (Fig. 3), the total pool available for recycling would be higher in OAV compared to CV and LAV. In fact, the lower acidification of the endosomal compartment in OAV, delaying the subsequent transfer to lysosome, would increase the amount of endosomal cargo at the superficial vesicles just below the apical membrane, forcing its transfer to the exocytosis pathway.

On the other hand, our results showed (Table 2) that the fluid and membrane-bound probes were not proportionally recycled. In fact, in all three diet-derived bladders, the membrane-bound probe recycled was higher than the fluid-probe recycled. Moreover, as shown in Table 3, the endocytosed membrane-bound probe and the V-ATPase activity (WAE $= 3.0$ and 2.75, respectively) prevailed over the other parameters in the OAV. These results may be partially supported by the evidences previously reported by Kreft′s group (2009). According to Kreft′s model, two pathways of internalization are possible: one from the urothelial plaques (carrying the UPIII as a possible targeting molecule to the lysosome; Bonifacino and Traub 2003) and the other from the hinge areas, containing most

of the fluid phase. Those authors concluded that contrary to the endocytosed membrane, the endocytosed fluid ends up in late endosome–lysosome without passing throughout the early endosomal compartment. Thus, our results may reflect the dichotomous origin of the vesicles and their internalization pathways followed by the probes in accordance, at least partially, with the model proposed by Kreft et al. (2009). Derganc et al. (2011) have theoretically analyzed the shape and structure of fusiform vesicles (FVs) in urinary bladder umbrella cells. They reported that the FVs, compartments with small volume-to-surface area ratio, ensure the membrane reinsertion at the apical surface with the minimal internalization of urine. This consideration may also be an alternative explanation for the difference between recycled fluid-probe and recycled membrane-bound probe reported by us (Fig. 9). Furthermore, the same difference is observed when analyzing the amount of fluid probe relative to the amount of membrane-bound probe that reaches the lysosomal compartment in CV and LAV (Figs. 7, 8). On these bases, it seems reasonable to infer that the change in lipid composition in OAV would alter the endocytosed vesicle shape, increasing the volume-to-surface area ratio, leading to a higher recycling (both fluid and membrane) and lysosomal pathway as well as to an increased leakage relative to CV and LAV (Table 2). In conclusion, the lower colocalization of both fluid and membrane-bound probes with lysosomal marker and the higher recycling of the probes observed in OAV suggest the displacement of this type of vesicles from the degradation pathway to the recycling cycle.

The results shown in Table 2, where the probe transferred to the cytosol (leakage) previously reported (Grasso and Calderón 2009), indicate that the fluid probe retained in the different compartments of oleic acid umbrella cells reached about 90 %, while the membrane-bound probe was about 70 % of the total endocytosed probe. Retention of fluid probe in oleic acid umbrella cells is mainly in the cytosol, while the membrane-bound probe is in the lysosome. The cytosolic retention could have negative effects on the umbrella cells' normal physiology, especially considering the possible presence of toxic elements (excreted by the urine) such as arsenic. In effect, arsenic is able to induce membrane permeabilization of the urothelial endocytic vesicles (Grasso et al. 2011b) and thus increase the risk of delivering not only arsenic, but also other toxic substances to the cytoplasm, avoiding their transfer to the lysosome and their possible degradation.

Conclusion

The membrane lipid composition of urinary umbrella cells shows a critical role for determining the amount of endocytosed material and its intracellular fate. Clear differences were observed in the traffic of both fluid probe and membrane-bound probe in urothelial umbrella cells with different membrane lipid compositions established by dietary treatments. The distinguished pattern of endocytic vesicles derived from oleic acid-enriched diet (OAV) shows both lower endocytosis capacity and delivery to the lysosome in comparison to those derived from linoleic acid and control diets (LAV and CV). The higher intravesicular pH and the impairment of the lysosomal pathway of OAV compared to LAV and CV correlate with the lower V-ATPase activity previously reported by us (Grasso et al. 2011a). Simultaneously, the higher exocytosis and the lower lysosomal pathway observed in OAV in relation to LAV and CV seem to reflect the displacement of the lysosomal pathways toward the exocytosis pathway, suggesting how membrane lipid composition/organization may regulate the balance between membrane internalization and membrane reinsertion.

Acknowledgments This work was supported by grants from SECYT-UNC and CONICET, Argentina. E.J. Grasso is a postdoctoral fellow of CONICET, Argentina. Confocal microscopy analyses were performed in the Microscopy Laboratory located in CIQUIBIC UNC, Córdoba, Argentina. We are grateful to Dr. Bruno Maggio for the careful revision of the manuscript.

References

Apodaca G (2004) The uroepithelium: not just a passive barrier. Traffic 5:117–128

Baenziger JE, Jarrell HC, Hill RJ, Smith IC (1991) Average structural and motional properties of a diunsaturated acyl chain in a lipid bilayer: effects of two cis-unsaturated double bonds. Biochemistry 30:894–903

Bongiovanni GA, Eynard AR, Calderón RO (2005) Altered lipid profile and changes in uroplakin properties of rat urothelial plasma membrane with diets of different lipid composition. Mol Cell Biochem 271:69–75

Bonifacino JS, Traub LM (2003) Signals for sorting of transmembrane proteins to endosomes and lysosomes. Annu Rev Biochem 72:395–447

Calderón RO, Eynard AR (2000) Fatty acids specifically related to anisotropic properties of plasma membranes from rat urothelium. Biochem Biophys Acta 1483:174–184

Calderón RO, Grasso EJ (2006) Symmetric array of the urothelium surface controlled by the lipid lattice composition. Biochim Biophys Res Commun 339:642–646

Calderón RO, Glocker M, Eynard AR (1998) Lipid and fatty acid composition of different fractions from rat urinary transitional epithelium. Lipids 33:1017–1022

Chang A, Hammond T, Sun TT, Zeidel M (1994) Permeability properties of the mammalian bladder apical membrane. Am J Physiol 267:C1483–C1492

Cipriano DJ, Wang Y, Bond S, Hinton A, Jefferies KC, Qi J, Forgac M (2008) Structure and regulation of the vacuolar ATPases. Biochim Biophys Acta 1777:599–604

Cohen SM (2002) Comparative pathology of proliferative lesions of the urinary bladder. Toxicol Pathol 30:663–671

Derganc J, Božič B, Romih R (2011) Shapes of discoid intracellular compartments with small relative volumes. PLoS ONE 6(11): e26824

Funari SS, Barceló F, Escribá PV (2003) Effects of oleic acid and its congeners, elaidic and stearic acids, on the structural properties of phosphatidylethanolamine membranes. J Lipid Res 44: 567–575

Grasso EJ, Calderón RO (2009) Urinary bladder membrane permeability differentially induced by membrane lipid composition. Mol Cell Biochem 330:163–169

Grasso EJ, Bongiovanni GA, Perez RD, Calderón RO (2011a) Precancerous changes in urothelial endocytic vesicles leakage, fatty acid composition and As and associated element concentrations after arsenic exposure. Toxicology 284:26–33

Grasso EJ, Scalambro MB, Calderón RO (2011b) Differential response of the urothelial V-ATPase activity to the lipid environment. Cell Biochem Biophys 61:157–168

Guo X, Tu L, Gumper I, Plesken H, Novak EK, Chintala S, Swank RT, Pastores G, Torres P, Izumi T, Sun TT, Sabatini DD, Kreibich G (2009) Involvement of Vps33a in the fusion of uroplakin-degrading multivesicular bodies with lysosomes. Traffic 10:1350–1361

Hicks RM (1975) The mammalian urinary bladder: an accommodating organ. Biol Rev 50:215–246

Khandelwal P, Ruiz WG, Apodaca G (2010) Compensatory endocytosis in bladder umbrella cells occurs through an integrin-regulated and RhoA- and Dynamin-dependent pathway. EMBO J 29:1961–1975

Kreft M, Milisav I, Potokar M, Zorec R (2004) Automated high through-put colocalization analysis of multichannel confocal images. Comp Meth Progr Biomedicine 74:63–67

Kreft ME, Romih R, Kreft M, Jezernik K (2009) Endocytotic activity of bladder superficial urothelial cells is inversely related to their differentiation stage. Differentiation 77:48–59

Lee AG (2004) How lipids affect the activities of integral membrane proteins. Biochim Biophys Acta 1666:62–87

Lewis SA (2000) Everything you wanted to know about the bladder epithelium but were afraid to ask. Am J Physiol 278:F867–F874

Lewis SA, de Moura J (1984) Apical membrane area of rabbit urinary bladder increases by fusion of intracellular vesicle: an electrophysiological study. J Membr Biol 82:123–136

Lowry ROH, Rosebrough NJ, Farr AL, Randall RJ (1951) Protein measurement with the Folin phenol reagent. J Biol Chem 193:265–275

Mahoney EM, Hamill AL, Scott WA, Cohn ZA (1997) Response of endocytosis to altered fatty acyl composition of macrophage phospholipids. Proc Natl Acad Sci USA 74:4895–4899

Marshansky V, Futai M (2008) The V-type H+ -ATPase in vesicular trafficking: targeting, regulation and function. Curr Opin Cell Biol 20:415–426

Mason JT, Huang C, Biltonene RL (1981) Calorimetric investigations of saturated mixed-chain phosphatidylcholine bilayer dispersions. Biochemistry 20:6086–6092

Nagle JF, Tristam-Nagle S (2000) Structure of lipids bilayers. Biochim Biophys Acta 1469:159–195

Perez Bay AE, Belingheri AV, Alvarez YD, Marengo FD (2011) Membrane cycling after the excess retrieval mode of rapid endocytosis in mouse chromaffin cells. Acta Physiol (Oxf) 204(3):403–418

Romih R, Jezernik K (1994) Endocytosis during postnatal differentiation in superficial cells of the mouse urinary bladder. Cell Biol Int 18(6):663–668

Straubinger RM, Papahadjopoulos D, Hong K (1990) Endocytosis and Intracellular fate of liposomes using pyranine as a probe. Biochemistry 29:4929–4939

Truschel ST, Wang E, Ruiz WG, Leung SM, Rojas R, Lavelle J, Zeidel M, Stoffer D, Apodaca G (2002) Stretch-regulated exocytosis/endocytosis in bladder umbrella cells. Mol Biol Cell 13:830–846

Wang Z, Lin H, Li C, Huang C (1995) Phase transition behavior and molecular structure of monounsaturated phosphatidylcholines. J Biol Chem 270:2014–2023

Wasungu L, Stuart MCA, Scarzello M, Engberts JBFN, Hoekstra D (2006) Lipoplexes formed from sugar-based Gemini surfactants undergo a lamellar-to-micellar phase transition at acidic pH. Evidence for a non-inverted membrane-destabilizing hexagonal phase of lipoplexes. Biochim Biophys Acta 1758:1677–1684

Zhang SX, Seguchi H (1994) The fate of the luminal asymmetric unit membrane of the superficial cell of the rat transitional epithelium. Histol Histopath 9:315–323

Zhou G, Liang FX, Romih R, Wang Z, Liao Y, Ghiso J, Luque-García JL, Neubert TA, Kreibich G, Alonso MA, Schaeren-Wiemers N, Sun TT (2012) MAL facilitates the incroporation of exocytic uroplakin-delivering vesicles into the apical membrane of urothelial umbrella cells. Mol Biol Cell 23(7):1354–1366